NeuroImage: Clinical 11 (2016) 339–346

Contents lists available at ScienceDirect

NeuroImage: Clinical

journal homepage: www.elsevier.com/locate/ynicl

Increased frontal functional networks in adult survivors of childhood brain tumors

Hongbo Chen[a,b,1], Liya Wang[a,c,1], Tricia Z. King[d,*], Hui Mao[a,**]

[a]Department of Radiology and Imaging Sciences, Emory University School of Medicine, Atlanta, GA, USA
[b]School of Life and Environmental Sciences, Guilin University of Electronic Technology, Guilin, Guangxi, China
[c]Department of Radiology, The Cancer Hospital of Chinese Academy of Medical Sciences, Shenzhen, Guangdong, China
[d]Department of Psychology and Neuroscience Institute, Georgia State University, Atlanta, GA, USA

ARTICLE INFO

Article history:
Received 18 November 2015
Received in revised form 13 February 2016
Accepted 18 February 2016
Available online 21 February 2016

Keywords:
Resting state fMRI
Functional connectivity
Brain tumor
Survivor

ABSTRACT

Childhood brain tumors and associated treatment have been shown to affect brain development and cognitive outcomes. Understanding the functional connectivity of brain many years after diagnosis and treatment may inform the development of interventions to improve the long-term outcomes of adult survivors of childhood brain tumors. This work investigated the frontal region functional connectivity of 16 adult survivors of childhood cerebellar tumors after an average of 14.9 years from diagnosis and 16 demographically-matched controls using resting state functional MRI (rs-fMRI). Independent component analysis (ICA) was applied to identify the resting state activity from rs-fMRI data and to select the specific regions associated with executive functions, followed by the secondary analysis of the functional networks connecting these regions. It was found that survivors exhibited differences in the functional connectivity in executive control network (ECN), default mode network (DMN) and salience network (SN) compared to demographically-matched controls. More specifically, the number of functional connectivity observed in the survivors is higher than that in the controls, and with increased strength, or stronger correlation coefficient between paired seeds, in survivors compared to the controls. Observed hyperconnectivity in the selected frontal functional network thus is consistent with findings in patients with other neurological injuries and diseases.

© 2016 The Authors. Published by Elsevier Inc. This is an open access article under the CC BY-NC-ND license (http://creativecommons.org/licenses/by-nc-nd/4.0/).

1. Introduction

Advances in diagnosis and treatment have led to improved clinical outcomes of pediatric brain tumor patients. The 5-year survival rate of these patients has increased from 55% in the 1970s to over 70% in more recent cohorts (Armstrong et al., 2009; Gurney et al., 2003; Ostrom et al., 2015). With improved treatment and longer survival, adult survivors of pediatric brain tumors are more than likely to experience adverse health and disrupted cognitive functions that may impact quality of life and cause social-economic difficulties (Gurney et al., 2009; Kirchhoff et al., 2011; Robinson et al., 2013). Currently, the specific neural and functional substrates associated with childhood brain tumor and its treatment are not well understood. Recently, we demonstrated that adult survivors of childhood brain tumors indeed exhibit altered brain activation during a working memory executive function task in a functional magnetic resonance imaging (fMRI) study (King et al., 2015a) and also reduced white matter integrity in the regions associated with intelligence in a diffusion tensor imaging (DTI) study (King et al., 2015b). These findings suggest the critical need for additional examination of the interruption or reorganization of connectivity among the regions involving the specific cognitive functions. Improved understanding of the functional and structural changes in adult survivors of childhood brain tumors may lead to new interventions helping to reduce the challenges survivors experience and improve their quality of life.

In the past several years, resting-state fMRI (rs-fMRI) has been increasingly used for mapping the functional connectivity of different brain regions. This non-invasive imaging technique offers unbiased analysis of the region to region interactions and connections at the functional level based on the rudimentary and intrinsic activity of the resting brain (Fox and Raichle, 2007; Friston, 2011). It has been widely applied to investigate the complex functional networks and changes during brain development and aging (Qi et al., 2014; Zhou et al., 2014) as well as alterations caused by diseases (van den Heuvel and Hulshoff Pol, 2010). Despite a rapidly expanding body of literature studying normal and disease affected brains through mapping functional connectivity with rs-fMRI, we still lack a clear understanding of the influence of

* Correspondence to: T. King, Department of Psychology, Georgia State University, P.O. Box 5010, Atlanta, GA 30302-5010, USA.
** Correspondence to: H. Mao, Department of Radiology and Imaging Sciences, Emory University School of Medicine, 1841 Clifton Road, Atlanta, GA 30329, USA.
E-mail addresses: tzking@gsu.edu (T.Z. King), hmao@emory.edu (H. Mao).
[1] These authors contributed to this work equally.

http://dx.doi.org/10.1016/j.nicl.2016.02.010
2213-1582/© 2016 The Authors. Published by Elsevier Inc. This is an open access article under the CC BY-NC-ND license (http://creativecommons.org/licenses/by-nc-nd/4.0/).

posterior fossa or cerebellar brain tumors on the cortical functional networks of adult survivors of childhood brain tumors.

In the present study, we hypothesize that functional and structural abnormalities observed in our early studies may lead to the disrupted or altered functional connectivity in the adult survivors of childhood brain tumors which can be examined by rs-fMRI. With the cohorts of adult survivors of childhood brain tumors and the demographically matched healthy controls who were included in our previous studies, we examined the triple unifying networks proposed by Menon and Uddin (2010). These three intrinsic connected networks are particularly important for understanding the brain connectivity at rest. This unifying networks include the executive control network (ECN), a frontoparietal cognitive system that controls and manages executive functions, such as working memory, and other cognitively demanding tasks that involve reasoning, planning and problem solving (Alvarez and Emory, 2006); default mode network (DMN), a set of brain regions that typically exhibit activations when an individual is in the state of wakeful rest (Broyd et al., 2009; Whitfield-Gabrieli and Ford, 2012) and is typically deactivated during most cognitive tasks, and is among the most commonly studied of the rs-fMRI analysis of connectivity networks; and salience network (SN), is the cingulate-frontal operculum system responsible for detecting and integrating "interoceptive, autonomic, and emotional" information (Menon and Uddin, 2010) and the coordination of behavioral responses (Medford and Critchley, 2010). These three RSNs have been shown to work synergistically in brain activations (Alexopoulos et al., 2012; Ham et al., 2013; Hellyer et al., 2014; Luo et al., 2014; Manoliu et al., 2014). Using the independent component analysis (ICA), a model-free approach for fMRI signal time course analysis, to identify and select the frontal regions that showed correlations in rs-fMRI data, functional connectivity analysis then revealed altered frontal functional networks, specifically increased functional connectivity, in adult survivors of pediatric brain tumors compared to the controls.

2. Materials and methods

2.1. Participants

The study was approved by the Georgia State University and Emory University Institutional Review Boards. Sixteen adult survivors of childhood brain tumors (10 females, age range: 17–34 years, mean age: 22.5, standard deviation: 5.2) participated in this study. All survivors were diagnosed and had been treated for pediatric cerebellar brain tumors on average 14.9 years prior to the exam (SD = 7.3), and on average at the age of 7.6 years (SD = 5.1). All participants were at least 7 years past their most recent diagnosis and treatment. They were recruited from a cohort of individuals who participated in an initial longitudinal childhood brain tumor study and later in the neuroimaging study (King et al., 2015a, 2015b). Written consent was obtained from all adult participants, while the parental written consent and participant assent were obtained from two individuals who were 17 years old. Information on the diagnosis of brain tumors and treatments was obtained from a retrospective review of the available medical records. None of the survivors included in this study was found to have a history of tumor progression or recurrence, neurofibromatosis or other significant neurological insult (e.g. stroke, traumatic brain injury or seizure). There is no indication of pervasive developmental disorders in these participants.

For comparison, sixteen healthy volunteers (10 females, age range: 18–34 years, mean age: 22.7, standard deviation: 4.1) were recruited as controls. The statistical analysis showed that the survivor and control subjects were matched in age ($p = 0.8816$, two sample two-tailed t-test) and gender ($p = 1$, chi-square test) with no statistically significant difference. Control participants were screened for current and history of neurological or developmental conditions and psychopathology based on the Structured Clinical Interview for DSM-IV-TR Axis 1 (First et al., 1997) to ensure that these individuals represented a healthy comparison group.

2.2. Resting state fMRI

MRI data were collected using a 3T Siemens Trio Tim MRI scanner with a 12-channel head coil. Participants were placed in the scanner in the supine position. Cushions and forehead straps were used to immobilize the head to minimize movement.

A routine clinical neuroimaging protocol, including diffusion weighted imaging, T_1-weighted spin echo and T_2-weighted FLAIR imaging was applied for each participant to ensure that there were no abnormal neuroradiology indications. In addition, T_1-weighted sagittal anatomic images with an isotropic resolution were acquired using a three-dimensional magnetization prepared rapid gradient echo (MP-RAGE) sequence with repetition time (TR) = 2250 ms, echo time (TE) = 3.98 ms, inversion time (TI) = 850 ms, flip angle (FA) = 9 degrees, matrix = 256 × 256, field of view (FOV) = 25.6 × 25.6 cm^2, slice thickness = 1.0 mm, no slice gap. Typically, a total of 176 slices were used to cover the whole brain.

During rs-fMRI data acquisition, participants were instructed to rest with their eyes open and looking at the crosshairs and keep their heads still during MRI scans. Blood oxygenation level-dependent (BOLD) image series were collected using a gradient-recalled T_2*-weighted echo-planar-imaging (EPI) sequence. The imaging parameters included: field of view of 240 mm, 40 slices, 3-mm slice thickness and no slice gap, TR = 2130 ms, TE = 30 ms, FA = 90 degrees giving a nominal resolution = 3 × 3 × 3 mm^3. The scan time of each rs-fMRI was 275 s, with a total of 129 volumes recorded.

2.3. Image processing and analysis

2.3.1. Data preprocessing

All rs-fMRI data were preprocessed using the software of Data Processing Assistant for Resting-State fMRI (DPARSF, http://www.restfmri.net/forum/DPARSF) (Chao-Gan and Yu-Feng, 2010) based on Statistical Parametric Mapping (SPM8, http://www.fil.ion.ucl.ac.uk/spm) and Resting-state fMRI Data Analysis Toolkit (REST, http://www.restfmri.net) (Song et al., 2011). All time course data were first evaluated for movement distortion and motion artifacts. The time course data were not included in the analysis if they exhibited displacement greater than 1.5 mm or rotation larger than 1.5° (Luo et al., 2014; Luo et al., 2012; Lou et al., 2014). There was no group difference in frame-wise head displacement after discarding data. In addition, the first 10 volumes of each time series of echo-planar images were discarded to minimize the effect of the un-equilibrium of tissue magnetization that may affect the BOLD signal (Burton et al., 2014; Liao et al., 2011). Thus, the remaining 119 time points of each time course image series were used for analysis. The selected time course images were subsequently corrected for slice timing and realigned to the image of the first time point for the correction of the rigid-body head movement. A band filter (0.01–0.08 Hz) installed in the "Functional Connectivity Toolkit" in the REST software was also applied to remove the low-frequency physiological noise. The time course images (3 × 3 × 3 mm^3) were then spatially normalized into the standard Montreal Neurological Institute (MNI) space, and smoothed using an isotropic Gaussian filter with full width at half maximum (FWHM) of 6 × 6 × 6 mm^3.

2.3.2. Independent component analysis (ICA) and component identification

Independent component analysis is well documented and applied in many statistical analyses literatures and research, although it has been increasingly applied to analyze imaging data in recent years. In contrast to traditional model-based fMRI data analysis, ICA offers a model-free, probability driven pattern or feature recognition approach. In our early study, we showed that using this model free approach is critical to capture the activation pattern or signal time course characteristics

that may be altered from normal hemodynamics due to disease or disease related reorganization (Wang et al., 2013). Conventional model based approaches may miss those features due to data correlation analysis using a pre-assumption model (or a model established from healthy population) to fit real data. ICA can capture signals from linear mixtures of these signals and then apply higher-order signal statistics to determine a set of "components" that are maximally independent of each other (Calhoun et al., 2013). Briefly, subject order independent group ICA (SOI-GICA) was conducted for all 32 participants using the infomax algorithm (Bell and Sejnowski, 1995) and the program (http://www.nitrc.org/projects/cogicat) (Zhang et al., 2010) Each calculation was done with a randomized initial value and a different subject order. In the typical group ICA approach, the analysis is done first by concatenating the individual data across time, followed by computing the subject-specific components and time courses. In the present study, we adopted the strategy of SOI-GICA, and performed group ICA 100 times, resulting in 30 independent components (ICs). The individual-level components were obtained from back-reconstruction and converted into z scores which reflect the correlation of BOLD signal time courses in a given voxel (Liang et al., 2014).

To verify the reproducibility of the ICs obtained from the ICA, two separate group ICA were carried out using the data from the survivor group and control group to ensure that the resulting components of the two groups had similar resting state fluctuations to those components obtained from using the data combined all 32 participants (Jafri et al., 2008). The reproducibility of ICs was further tested using the analysis of decomposition of 20, 30 and 40 components, respectively, to confirm the stability of the selected components.

To ensure the selected components contained the brain regions showing the resting state activity for further functional connectivity analysis, we compared the probabilistic maps of each IC with spatial maps of gray matter, white matter, and cerebral spinal fluid (CSF) within the standard brain space (MNI templates provided in SPM2). The ICs with probabilistic maps showing the resting state activity patterns largely presented in the gray matter were selected (Stevens et al., 2007). Components with probabilistic maps in the space of CSF or white matter were considered as possible artifacts even though they may exhibit high correlations. Correlation analysis indicated that no IC in the current study showed a probabilistic map in the white matter space (Stevens et al., 2007). Visual inspection of discarded components suggested that they were likely related to eye movement, head motion, or heart-beat induced cerebral pulsation.

2.3.3. Selection of the regions of interest for functional connectivity analysis

In this study, the areas showing resting-state activations in ICs identified by ICA were then used to select the regions of interest or seeds for further functional connectivity analysis. First, we selected the ICs based on prior knowledge of brain regions that are considered to be part of the executive control functional network (Dong et al., 2015; Krmpotich et al., 2013), and salience network (Medford and Critchley, 2010; Menon and Uddin, 2010) as well as default-mode network (Broyd et al., 2009; Whitfield-Gabrieli and Ford, 2012) that are commonly reported in the resting state network literature. Because the executive control network (ECN) has been shown to have separable right and left hemisphere components, and the default-mode network (DMN) includes anterior-dominant and posterior-dominant components (Jones et al., 2011), we selected five ICs containing those regions for further analysis, i.e., the left ECN (LECN), the right ECN (RECN), the anterior-dominant DMN (ADMN), the posterior-dominant DMN (PDMN), and SN.

Each selected IC was then given its own mask generated based on the respective network reported in the literature using the REST Image Calculator Toolkit in the REST software (REST, http://www.restfmri.net) (Song et al., 2011). The masks for the selected ICs should contain the group-level resting state activity patterns in survivors and controls that were generated for survivors and controls separately using one sample t-tests. Although resting state activity patterns observed in the survivor and control groups may have different sizes and not overlap (Correa et al., 2007), the mask for each selected IC covers the resting state activity patterns of both groups.

The next step of the pre-process used the voxel-wise two sample t-test analysis on Z maps of each IC to obtain significant differences between the two groups. The inter-group comparison was restricted to the voxels in the masks for each RSN. ROIs were then identified as clusters consisting of contiguously significant voxels with a threshold $p < 0.01$ ($|T| > 2.75$). These clusters were tested for cluster-level family wise error (FWE) correction ($p < 0.01$) and the AlphaSim estimation (Dong et al., 2015). The selected ROIs were used as seeds to the subsequent functional network analysis (Liao et al., 2011). A total of 11 ROIs were selected from 5 RSN specifically associated with the executive control network (ECN) and DMN.

2.3.4. Calculation of functional connectivity

We used functional connectivity to identify distinct networks in the frontal regions of adult survivors. Functional connectivity was defined as the statistically significant temporal correlation coefficients of resting-state BOLD signal time courses recorded in two "pairing" ROIs or seeds. The Functional Connectivity Toolkit in the REST software (REST) was used to compute the FC in all participants. The BOLD signal time courses of each selected ROI used for temporal correlation computations were the averaged BOLD signals from the voxels in a 5-mm-radius sphere centered on the location with the maximal t-value in the t-map after t-test analysis (Shankman et al., 2014). Functional connectivity in individual paired ROIs was calculated using the 119 time point rs-fMRI data (Andrews-Hanna et al., 2010; Burton et al., 2014; Liao et al., 2011). The strength of FC was defined as the statistically significant temporal correlation coefficients of resting-state BOLD signal time courses recorded in two "pairing" brain regions or ROIs using the temporal Pearson correlation analysis.

2.3.5. Statistical analysis

To evaluate FC within each group, one sample t-test ($p < 0.01$) was carried out on each pair of ROIs in the survivor and control groups, respectively. When the average correlation coefficient between a pair of ROIs was greater than 0.3 (Buckner et al., 2009), it was considered that there is a significant or between-group FC differences between two brain regions. Then, we compared the FC using the number of FC in each group. The graphical presentations of the FCs in each group and their significant differences between the two groups were generated using BrainNet Viewer (http://www.nitrc.org/projects/bnv).

Using two sample t test to compare the functional connectivity observed from the survivors and controls, the between-group differences ($p < 0.05$) in functional connectivity were identified. These statistically significant differences were graphically displayed using The BrainNet Viewer (http://www.nitrc.org/projects/bnv).

3. Results

3.1. Resting state functional networks in adult survivors of pediatric brain tumors

After we excluded all the data with motion artifacts above the screening criteria indicated above, we found no group difference in frame-wise head displacement (Power et al., 2015). The analysis of rs-fMRI data using the described procedure yielded the functional network information of the survivor and control groups. Fig. 1 shows the selected components representing several selected regions of RSN (labeled as RSN1 to RSN5). RSN1 appears to be a part of the right executive control network (R-ECN), which consisted of the middle frontal gyrus, the superior frontal gyrus, the inferior frontal gyrus, the sub-gyral, the medial frontal gyrus, the superior temporal gyrus, the middle temporal gyrus, the postcentral gyrus, precuneus and the precentral gyrus. RSN2 is

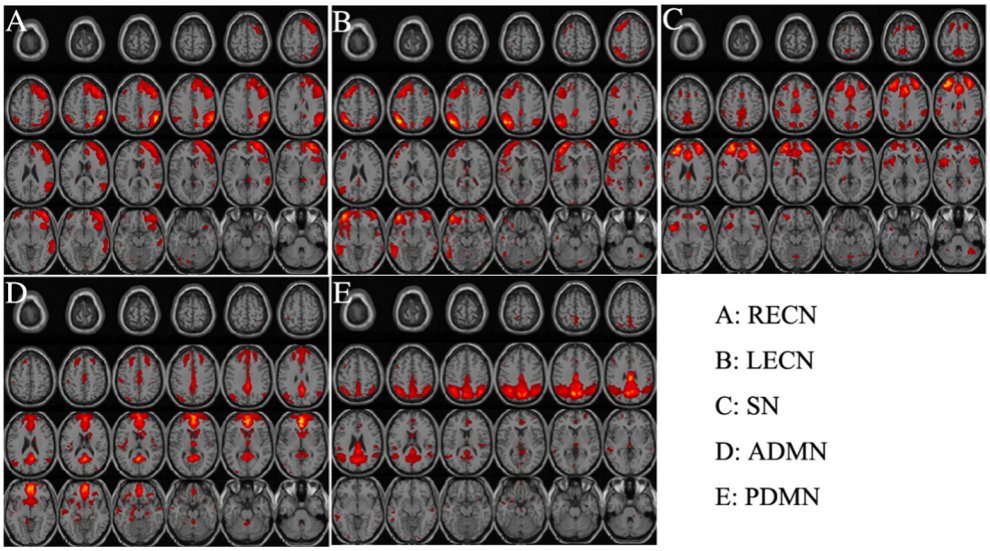

Fig. 1. Maps of resting state activity patterns of five independent components were used for analysis of functional connectivity. A–E: RECN = right executive control network; LECN = left executive control network; SN = salience network; ADMN = anterior default-mode network; PDMN = posterior default-mode network.

part of the left executive control network (L-ECN), involving the sub-gyral, the middle frontal gyrus, superior frontal gyrus, middle temporal gyrus, superior temporal gyrus, inferior frontal gyrus, inferior parietal lobule, medial frontal gyrus, precuneus, the precentral gyrus, the cingulate gyrus and the postcentral gyrus. RSN3 was selected for its relationship to the salience network (SN) that includes the middle frontal gyrus, sub-gyral, superior frontal gyrus, precuneus, medial frontal gyrus, inferior frontal gyrus, precentral gyrus, superior temporal gyrus and insula. RSN4 and RSN5 are anterior (A-DMN) and posterior (P-DMN) portions of default-mode network, respectively. A-DMN involves the superior frontal gyrus, middle frontal gyrus, medial frontal gyrus, cingulate gyrus, sub-gyral, middle temporal gyrus, inferior frontal gyrus, insula, superior temporal gyrus and the middle occipital gyrus. P-DMN mainly includes the precuneus, sub-gyral, middle temporal gyrus, cingulate gyrus, superior temporal gyrus, cuneus, middle frontal gyrus, postcentral gyrus, and medial frontal gyrus.

The spatial match of those selected ICs to the template of functional anatomy (http://findlab.stanford.edu/functional_ROIs.html) using correlation analysis (Franco et al., 2009; Krmpotich et al., 2013) indicated that there is a statistically significant similarity, i.e., correlation coefficient > 0.35, between the template and the ICs within the selected networks R-ECN (0.4062), L-ECN (0.4909), SN (0.3883), A-DMN (0.6328) and P-DMN (0.5094).

3.2. Altered functional networks in adult survivors of pediatric brain tumors

The two-sample t-test comparison analysis of RSNs between the survivor and control groups revealed statistically significant differences in all five selected frontal functional networks. Overall, 11 ROIs, as shown in Fig. 2, exhibited statistically significant differences between the two groups, including 3 ROIs in R-ECN, 2 in L-ECN, 1 in SN, and 5 in A-DMN. However, no significant difference was found in ROIs within P-DMN. The details on each ROI are summarized in Table 1.

Furthermore, increased z-scores were found in 7 ROIs in survivors compared with controls. They are located in the right middle frontal gyrus, right postcentral gyrus, left inferior frontal gyrus, left putamen, right/left superior frontal gyrus, and insula. These regions are related to the Brodmann area (BA) 9, 10, 2, 47 and 48. The other 4 ROIs exhibited decreased z-scores in survivors compared with controls. They are located in the right superior frontal gyrus, left supplementary motor area, anterior cingulum, caudate nucleus or BA 9, 6, 32, 11, 25.

3.3. Reorganization of functional connectivity in adult survivors of pediatric brain tumors

Given the functional networks presented above, we further examined the reorganization of functional connectivity in survivors in terms of the number of connected areas and the extent of the activation in these connected regions. Fig. 3 shows the averaged numbers of FC in survivors and controls (i.e., correlation coefficients greater than 0.3), respectively. There are 10 FCs observed in controls. In comparison, there are 25 FCs observed in the survivor group.

In addition to the observation of increased number of FCs in the frontal region of the survivor group, it is also noticed that the strength of FCs, defined as the level of the correlation coefficients obtained from seed-paired FC analysis, in the selected frontal regions are also different between the survivor and control groups as shown in the correlation maps in Fig. 4. The survivors generally exhibited increased FC strength or higher correlation coefficient.

Furthermore, we found three FCs that had statistically significant differences between survivors and controls. All these FCs exhibiting between-group difference were located within the RECN network or between RECN and SN (Fig. 5) with the strength of FCs in survivors higher than that in controls.

4. Discussion

Early studies, including ours, have revealed that adult survivors of childhood cerebellar tumors and subsequent treatment had lower white matter integrity in the several frontal brain regions that correlated with lower intelligence. Most recently we have found that there are significantly greater levels of percent signal change in the blood oxygenation level dependent (BOLD) activations of the left prefrontal lobe and left parietal lobe in adult survivors relative to a healthy demographically-similar control group during a verbal working memory task (King et al., 2015a). These results suggested that the cognitive demands of the more challenging working memory tasks are specifically associated with these increased regions of hemodynamic response and not overall differences in cognitive ability. Increased prefrontal cortex activation during working memory tasks, as working memory performance declines, has been reported previously in the literature with various neurological populations. The *allocation of latent resources theory* of the prefrontal lobe was

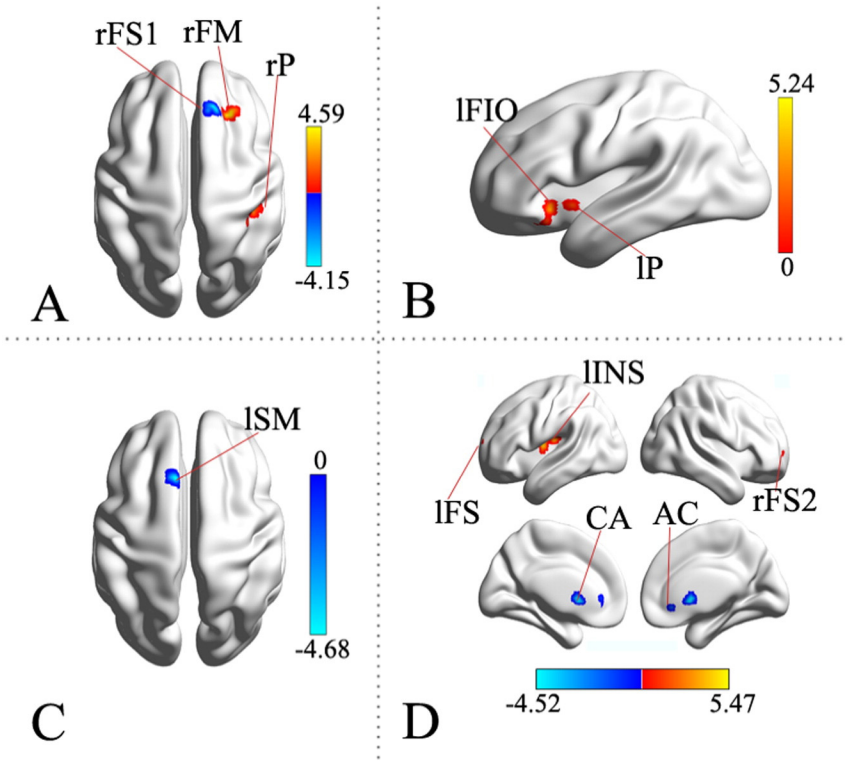

Fig. 2. The cortical regions within the selected RSNs that showed statistically significant differences in FC between the survivors and controls (two-sample t-test, $p < 0.01$ corrected). The orange-yellow colors indicate the brain regions with significantly increased z-score in survivors compared with controls, while blue color indicates decreased z-score in survivors. A. right executive control network (RECN); B. Left executive control network (LECN); C. Salience network (SN); D. Anterior default-mode network (ADMN). rFM, rP, rFS1, AC, CA, rFS2, lFS, lINS, lSM, lFIO, lP are the ROIs that were described in Table 1. The images were prepared with the BrainNet Viewer (http://www.nitrc.org/projects/bnv). (For interpretation of the references to color in this figure legend, the reader is referred to the web version of this article.)

proposed to describe when prefrontal BOLD response increases with greater task demands.

The current functional connectivity study found that long-term survivors of childhood brain tumors exhibited increased strength and number of functional connectivity in the executive control network (ECN), default mode network (DMN) and salience network (SN) compared to a demographically-matched comparison group supports this notion with evidence of increased number and strength of functional connectivities in the selected frontal networks of adult survivors. This finding might imply that continuous needs of a higher level of effort by survivors may result in recruiting more brain regions through connectivity of the frontal functional networks. The hyperconnectivity during

Table 1
Regions showing different resting state activity patterns between survivors and controls.

	ROI	x,y,z[a]	Peak t value[b]	Number of voxels[c]	BA[d]	Region[e]	Hemi sphere
ROIs in RECN							
1	rFM	27,30,39	+3.22	13	9	Middle frontal	R
2	rP	42,−30, 48	+4.59	13	2	Postcentral	R
3	rFS1	15, 36,51	−4.15	10	9	Superior frontal	R
ROIs in LECN							
4	lFIO	−30, 24, −15	+5.24	20	47	Inferior frontal	L
5	lP	−18,3, 9	+4.56	23	48	Putamen	L
ROI in SN							
6	lSM	−9, 21, 60	−4.68	21	6	Supplementary motor	L
ROIs in ADMN							
7	AC	0,33, −6	−3.52	20	32,11	Anterior cingulum	L/R
8	CA	0, 9, 3	−4.52	21	25	Caudate	L/R
9	rFS2	30, 63, 9	+3.74	20	10	Superior frontal	R
10	lFS	−30, 66, 15	+3.63	14	10	Superior frontal	L
11	lINS	−36, −6, 12	+5.47	58	48	Insula	L

No Significant difference ROI in PDMN.

[a] Peak coordinates of MNI brain atlas. MNI = Montreal Neurological Institute.

[b] The peak t value, '+' indicates the increased z-score in survivors, and '-' indicates the decreased z-score in survivors.

[c] These clusters were tested for cluster-level FWE correction $p < 0.01$ and the AlphaSim estimation indicated that clusters with 10 contiguous voxels would achieve an effective FWE threshold $p < 0.01$ in RSN1, and 13, 13, 11 in RSN2, RSN3, RSN4, respectively. Voxel size = 3 × 3 × 3.

[d] Brodmann's area, double checked with the xjview software ((http://www.alivelearn.net/xjview/).

[e] The brain regions were referenced to the Automated Anatomical Labeling (AAL), and also double checked with the xjview software.

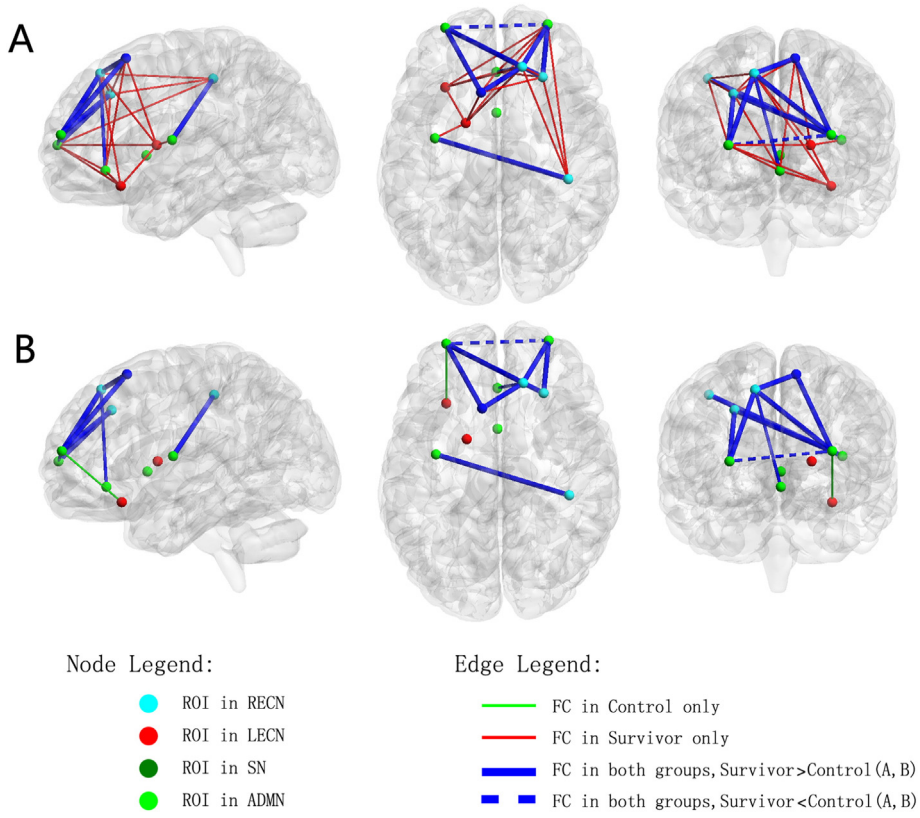

Fig. 3. Functional connectivity in the frontal areas of survivor and control groups. The nodes represent the ROIs extracted from the selected RSNs; the edges represent the FCs between pairs of nodes which are connected (FC strength > 0.3). A. connected regions found in controls; B. The connected regions observed in controls. FC = functional connectivity; ROI = region of interest; RECN = right executive control network; LECN = left executive control network; SN = salience network; ADMN = anterior default-mode network. Images were prepared with the BrainNet Viewer (http://www.nitrc.org/projects/bnv).

rs-fMRI is consistent with studies of other neurological injuries and disease. Such hyperconnectivity perhaps is eliciting an "all hands on deck" approach even at rest.

As far as the method using rs-fMRI based functional connectivity analysis, there are two common approaches, i.e., 1) using the signal time courses from regions of interest as the seeds to explore the connected brain regions based on the correlations of these signal time courses in the seeds to other areas within the network; 2) using the a priori known components of functional network as the masks to "determine" the regions within the mask based on levels of statistical significance of the correlations between the time courses of those regions within defined networks. In our study, we used ICA for exploring the functional connectivity at the resting state. ICA has the ability to reveal inter-event and inter-subject differences in the temporal dynamics (Calhoun et al., 2003), and it was successfully applied to identify resting-state networks according to human cognitive activity, such as the default mode network (Cowdrey et al., 2014; Liang et al., 2014), executive control network (Jukuri et al., 2015; Littow et al., 2015; Manoliu et al., 2014), salience network (Thome et al., 2014), and motor network (Amadi et al., 2013; Dipasquale et al., 2015). We chose to use the ICA approach given its probability emphasized statistical analysis, therefore, allowing for relatively unbiased selecting and "recommending" the

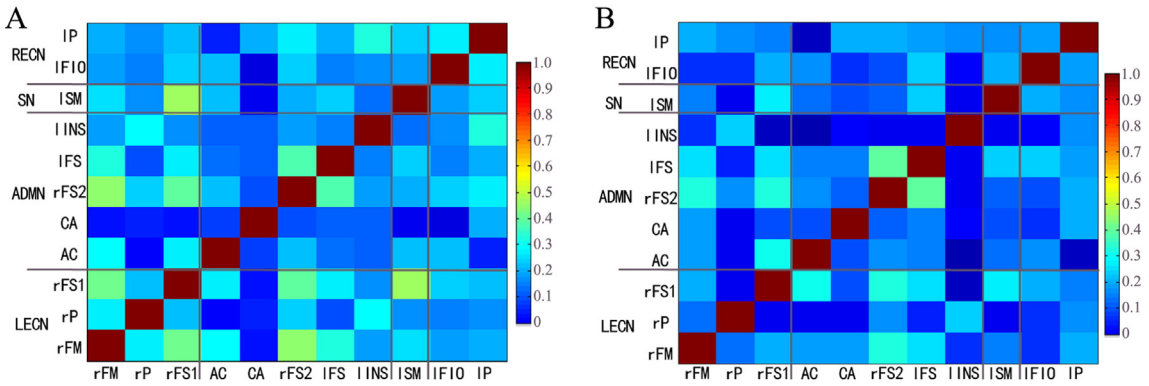

Fig. 4. Color-coded maps showing the level of the correlation coefficients of functional connectivity calculated from paired ROIs. A. Survivors; B. Controls. The higher correlation coefficients were found in the many regions of the survivor group comparing to the control group. ROIs shown in the maps are: RECN = right executive control network; LECN = left executive control network; SN = salience network; ADMN = anterior default-mode network. rFM, rP, rFS1, AC, CA, rFS2, lFS, lINS, lSM, lFIO, IP are the ROIs that were described in Table 1. (For interpretation of the references to color in this figure legend, the reader is referred to the web version of this article.)

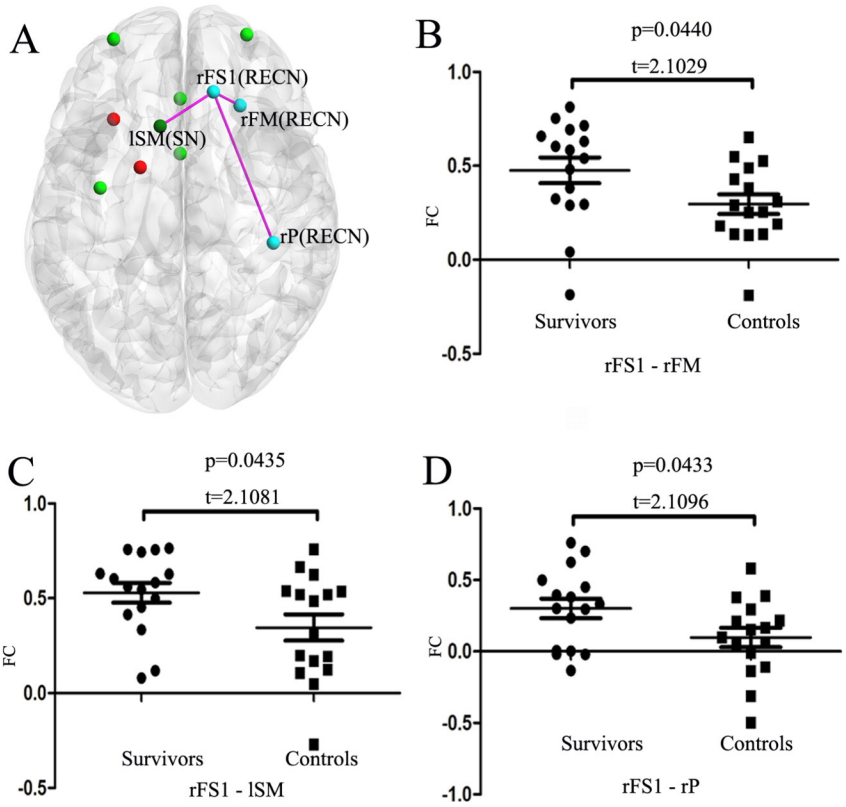

Fig. 5. The FCs that have statistically significant difference between survivors and controls based on two sample t-test ($p < 0.05$). A. The significantly different FCs visualized with the BrainNet Viewer. The scatter plot for FC between ROIs rFS1 and rFM (B); ROIs rFS1 and lSM (C); and ROIs rFS1 and rP (D), which have significant differences. FC = functional connectivity; RECN = right executive control network; SN = salience network. rFM, rP, rFS1, lSM are the selected ROIs that were described in Table 1.

possible regions for subsequent seed-based FC analysis. The selection of ROIs can directly influence the analysis and results of functional MRI data and connectivity. Conventional approaches for FC analysis select the ROIs or seeds based on the commonly used functional network atlas established using healthy controls (Alonso-Solis et al., 2015; Craddock et al., 2009; Dong et al., 2015; Nair et al., 2014). However, it is possible that the hemodynamics and brain region may differ in adult survivors of childhood brain tumors compared to healthy controls, with concerns of potentially inducing selection bias (Cordes et al., 2000; Damoiseaux and Greicius, 2009), Thus, our rationale is that use of ICA approach to select ROIs or seeds that have significant differences between survivors and controls in the known RSNs for FC analysis may minimize the bias introduced by the priori knowledge.

Acknowledgment

We would like to express our gratitude to the individuals and families who participated in this study and generously contributed their time and effort. This research was supported in part by a Research Scholar Grant from the American Cancer Society to TZK (#RSGPB-CPPB-114044), a project grant from the National Natural Science Foundation of China to HC (81460273) and a research grant from National Cancer Institute to HM (5R01CA169937-01A1). Authors also thank Miss. Jessica Paulishen for her assistance in editing and proofreading the manuscript.

Appendix A. Supplementary data

Supplementary data to this article can be found online at http://dx.doi.org/10.1016/j.nicl.2016.02.010.

References

Alexopoulos, G.S., Hoptman, M.J., Kanellopoulos, D., Murphy, C.F., Lim, K.O., Gunning, F.M., 2012. Functional connectivity in the cognitive control network and the default mode network in late-life depression. J. Affect. Disord. 139, 56–65.
Alonso-Solis, A., Vives-Gilabert, Y., Grasa, E., Portella, M.J., Rabella, M., Sauras, R.B., Roldan, A., Nunez-Marin, F., Gomez-Anson, B., Perez, V., Alvarez, E., Corripio, I., 2015. Resting-state functional connectivity alterations in the default network of schizophrenia patients with persistent auditory verbal hallucinations. Schizophr. Res. 161, 261–268.
Alvarez, J.A., Emory, E., 2006. Executive function and the frontal lobes: a meta-analytic review. Neuropsychol. Rev. 16, 17–42.
Amadi, U., Ilie, A., Johansen-Berg, H., Stagg, C.J., 2013. Polarity-specific effects of motor transcranial direct current stimulation on fMRI resting state networks. NeuroImage 88C, 155–161.
Andrews-Hanna, J.R., Reidler, J.S., Sepulcre, J., Poulin, R., Buckner, R.L., 2010. Functional-anatomic fractionation of the brain's default network. Neuron 65, 550–562.
Armstrong, G.T., Liu, Q., Yasui, Y., Huang, S., Ness, K.K., Leisenring, W., Hudson, M.M., Donaldson, S.S., King, A.A., Stovall, M., Krull, K.R., Robison, L.L., Packer, R.J., 2009. Long-term outcomes among adult survivors of childhood central nervous system malignancies in the childhood cancer survivor study. J. Natl. Cancer Inst. 101, 946–958.
Bell, A.J., Sejnowski, T.J., 1995. An information-maximization approach to blind separation and blind deconvolution. Neural Comput. 7, 1129–1159.
Broyd, S.J., Demanuele, C., Debener, S., Helps, S.K., James, C.J., Sonuga-Barke, E.J., 2009. Default-mode brain dysfunction in mental disorders: a systematic review. Neurosci. Biobehav. Rev. 33, 279–296.
Buckner, R.L., Sepulcre, J., Talukdar, T., Krienen, F.M., Liu, H., Hedden, T., Andrews-Hanna, J.R., Sperling, R.A., Johnson, K.A., 2009. Cortical hubs revealed by intrinsic functional connectivity: mapping, assessment of stability, and relation to Alzheimer's disease. J. Neurosci. 29, 1860–1873.
Burton, H., Snyder, A.Z., Raichle, M.E., 2014. Resting state functional connectivity in early blind humans. Front. Syst. Neurosci. 8, 51.
Calhoun, V.D., Adali, T., Hansen, L.K., Larsen, J., Pekar, J.J., 2003. ICA of functional MRI data: an overview. Proceedings of the 4th International Symposium ICA2003, pp. 281–288.
Calhoun, V.D., Potluru, V.K., Phlypo, R., Silva, R.F., Pearlmutter, B.A., Caprihan, A., Plis, S.M., Adalı, T., 2013. Independent component analysis for brain fMRI does indeed select for maximal independence. PLoS One 8, 1–8.
Chao-Gan, Y., Yu-Feng, Z., 2010. DPARSF: a MATLAB toolbox for "Pipeline" data analysis of resting-state fMRI. Front. Syst. Neurosci. 4, 13.
Cordes, D., Haughton, V.M., Arfanakis, K., Wendt, G.J., Turski, P.A., Moritz, C.H., Quigley, M.A., Meyerand, M.E., 2000. Mapping functionally related regions of brain with functional connectivity MR imaging. Am. J. Neuroradiol. 21, 1636–1644.

Correa, N., AdalV, T., Calhoun, V.D., 2007. Performance of blind source separation algorithms for fMRI analysis using a group ICA method. Magn. Reson. Imaging 25, 1–18.
Cowdrey, F.A., Filippini, N., Park, R.J., Smith, S.M., McCabe, C., 2014. Increased resting state functional connectivity in the default mode network in recovered anorexia nervosa. Hum. Brain Mapp. 35, 483–491.
Craddock, R.C., Holtzheimer III, P.E., Hu, X.P., Mayberg, H.S., 2009. Disease state prediction from resting state functional connectivity. Magn. Reson. Med. 62, 1619–1628.
Damoiseaux, J.S., Greicius, M.D., 2009. Greater than the sum of its parts: a review of studies combining structural connectivity and resting-state functional connectivity. Brain Struct. Funct. 213, 525–533.
Dipasquale, O., Griffanti, L., Clerici, M., Nemni, R., Baselli, G., Baglio, F., 2015. High-dimensional ICA analysis detects within-network functional connectivity damage of default-mode and sensory-motor networks in Alzheimer's disease. Front. Hum. Neurosci. 9, 43.
Dong, G., Lin, X., Potenza, M.N., 2015. Decreased functional connectivity in an executive control network is related to impaired executive function in Internet gaming disorder. Prog. Neuro-Psychopharmacol. Biol. Psychiatry 57, 76–85.
First, M.B., Spitzer, R.L., Gibbon, M., Williams, J.B.W., 1997. Structured Clinical Interview for DSM-IV Axis 1 Disorders (SCID-I)-clinical version. American Psychiatric Publishing, Arlington, VA.
Fox, M.D., Raichle, M.E., 2007. Spontaneous fluctuations in brain activity observed with functional magnetic resonance imaging. Nat. Rev. Neurosci. 8, 700–711.
Franco, A.R., Pritchard, A., Calhoun, V.D., Mayer, A.R., 2009. Interrater and intermethod reliability of default mode network selection. Hum. Brain Mapp. 30, 2293–2303.
Friston, K.J., 2011. Functional and effective connectivity: a review. Brain Connect. 1, 13–36.
Gurney, J.G., Kadan-Lottick, N.S., Packer, R.J., Neglia, J.P., Sklar, C.A., Punyko, J.A., Stovall, M., Yasui, Y., Nicholson, H.S., Wolden, S., McNeil, D.E., Mertens, A.C., Robison, L.L., 2003. Endocrine and cardiovascular late effects among adult survivors of childhood brain tumors. Cancer 97, 663–673.
Gurney, J.G., Krull, K.R., Kadan-Lottick, N., Nicholson, H.S., Nathan, P.C., Zebrack, B., Tersak, J.M., Ness, K.K., 2009. Social outcomes in the childhood cancer survivor study cohort. J. Clin. Oncol. 27, 2390–2395.
Ham, T., Leff, A., de Boissezon, X., Joffe, A., Sharp, D.J., 2013. Cognitive control and the salience network: an investigation of error processing and effective connectivity. J. Neurosci. 33, 7091–7098.
Hellyer, P.J., Shanahan, M., Scott, G., Wise, R.J., Sharp, D.J., Leech, R., 2014. The control of global brain dynamics: opposing actions of frontoparietal control and default mode networks on attention. J. Neurosci. 34, 451–461.
Jafri, M.J., Pearlson, G.D., Stevens, M., Calhoun, V.D., 2008. A method for functional network connectivity among spatially independent resting-state components in schizophrenia. NeuroImage 39, 1666–1681.
Jones, D.T., Machulda, M.M., Vemuri, P., McDade, E.M., Zeng, G., Senjem, M.L., Gunter, J.L., Przybelski, S.A., Avula, R.T., Knopman, D.S., Boeve, B.F., Petersen, R.C., Jack, C.R., 2011. Age-related changes in the default mode network are more advanced in Alzheimer disease. Neurology 77, 1524–1531.
Jukuri, T., Kiviniemi, V., Nikkinen, J., Miettunen, J., Maki, P., Mukkala, S., Koivukangas, J., Nordstrom, T., Parkkisenniemi, J., Moilanen, I., Barnett, J.H., Jones, P.B., Murray, G.K., Veijola, J., 2015. Central executive network in young people with familial risk for psychosis–the oulu brain and mind study. Schizophr. Res. 161, 177–183.
King, T.Z., Na, S., Mao, H., 2015a. Neural underpinnings of working memory in adult survivors of childhood brain tumors. J. Int. Neuropsychol. Soc. 21, 494–505.
King, T.Z., Wang, L., Mao, H., 2015b. Disruption of white matter integrity in adult survivors of childhood brain tumors: correlates with long-term intellectual outcomes. PLoS One 10, 1–17.
Kirchhoff, A.C., Krull, K.R., Ness, K.K., Armstrong, G.T., Park, E.R., Stovall, M., Robison, L.L., Leisenring, W., 2011. Physical, mental, and neurocognitive status and employment outcomes in the childhood cancer survivor study cohort. Cancer Epidemiol. Biomark. Prev. 20, 1838–1849.
Krmpotich, T.D., Tregellas, J.R., Thompson, L.L., Banich, M.T., Klenk, A.M., Tanabe, J.L., 2013. Resting-state activity in the left executive control network is associated with behavioral approach and is increased in substance dependence. Drug Alcohol Depend. 129, 1–7.
Liang, P., Wang, Z., Qian, T., Li, K., 2014. Acupuncture stimulation of Taichong (Liv3) and Hegu (LI4) modulates the default mode network activity in Alzheimer's disease. Am. J. Alzheimers Dis. Other Demen. 29, 739–748.
Liao, W., Zhang, Z., Pan, Z., Mantini, D., Ding, J., Duan, X., Luo, C., Wang, Z., Tan, Q., Lu, G., Chen, H., 2011. Default mode network abnormalities in mesial temporal lobe epilepsy: a study combining fMRI and DTI. Hum. Brain Mapp. 32, 883–895.
Littow, H., Huossa, V., Karjalainen, S., Jaaskelainen, E., Haapea, M., Miettunen, J., Tervonen, O., Isohanni, M., Nikkinen, J., Veijola, J., Murray, G., Kiviniemi, V.J., 2015. Aberrant functional connectivity in the default mode and central executive networks in subjects with schizophrenia — a whole-brain resting-state ICA study. Front. Psychiatry 6, 26.
Luo, C., Qiu, C., Guo, Z., Fang, J., Li, Q., Lei, X., Xia, Y., Lai, Y., Gong, Q., Zhou, D., Yao, D., 2012. Disrupted functional brain connectivity in partial epilepsy: a resting-state fMRI study. PLoS One 7, e28196.
Luo, Y., Qin, S., Fernandez, G., Zhang, Y., Klumpers, F., Li, H., 2014. Emotion perception and executive control interact in the salience network during emotionally charged working memory processing. Hum. Brain Mapp. 35, 5606–5616.
Manoliu, A., Riedl, V., Zherdin, A., Muhlau, M., Schwerthoffer, D., Scherr, M., Peters, H., Zimmer, C., Forstl, H., Bauml, J., Wohlschlager, A.M., Sorg, C., 2014. Aberrant dependence of default mode/central executive network interactions on anterior insular salience network activity in schizophrenia. Schizophr. Bull. 40, 428–437.
Medford, N., Critchley, H.D., 2010. Conjoint activity of anterior insular and anterior cingulate cortex: awareness and response. Brain Struct. Funct. 214, 535–549.
Menon, V., Uddin, L.Q., 2010. Saliency, switching, attention and control: a network model of insula function. Brain Struct. Funct. 214, 655–667.
Nair, A., Keown, C.L., Datko, M., Shih, P., Keehn, B., Muller, R.A., 2014. Impact of methodological variables on functional connectivity findings in autism spectrum disorders. Hum. Brain Mapp. 35, 4035–4048.
Ostrom, Q.T., de Blank, P.M., Kruchko, C., Petersen, C.M., Liao, P., Finlay, J.L., Stearns, D.S., Wolff, J.E., Wolinsky, Y., Letterio, J.J., Barnholtz-Sloan, J.S., 2015. Alex's lemonade stand foundation infant and childhood primary brain and central nervous system tumors diagnosed in the United States in 2007–2011. Neuro-Oncology 16 (Suppl. 10), x1–x36.
Power, J.D., Schlaggar, B.L., Petersen, S.E., 2015. Recent progress and outstanding issues in motion correction in resting state fMRI. NeuroImage 105, 536–551.
Qi, R., Zhang, L.J., Xu, Q., Liang, X., Luo, S., Zhang, Z., Huang, W., Zheng, L., Lu, G.M., 2014. Abnormal functional connectivity within the default mode network in Patients with HBV-related cirrhosis without hepatic encephalopathy revealed by resting-state functional MRI. Brain Res. 1576, 73–80.
Robinson, K.E., Fraley, C.E., Pearson, M.M., Kuttesch Jr., J.F., Compas, B.E., 2013. Neurocognitive late effects of pediatric brain tumors of the posterior fossa: a quantitative review. J. Int. Neuropsychol. Soc. 19, 44–53.
Shankman, S.A., Gorka, S.M., Nelson, B.D., Fitzgerald, D.A., Phan, K.L., O'Daly, O., 2014. Anterior insula responds to temporally unpredictable aversiveness: an fMRI study. Neuroreport 25, 596–600.
Song, X.W., Dong, Z.Y., Long, X.Y., Li, S.F., Zuo, X.N., Zhu, C.Z., He, Y., Yan, C.G., Zang, Y.F., 2011. REST: a toolkit for resting-state functional magnetic resonance imaging data processing. PLoS One 6, e25031.
Stevens, M.C., Kiehl, K.A., Pearlson, G., Calhoun, V.D., 2007. Functional neural circuits for mental timekeeping. Hum. Brain Mapp. 28, 394–408.
Thome, J., Frewen, P., Daniels, J.K., Densmore, M., Lanius, R.A., 2014. Altered connectivity within the salience network during direct eye gaze in PTSD. Borderline Personal. Disord. Emot. Dysregul. 1, 17.
van den Heuvel, M.P., Hulshoff Pol, H.E., 2010. Exploring the brain network: a review on resting-state fMRI functional connectivity. Eur. Neuropsychopharmacol. 20, 519–534.
Wang, L., Chen, D., Yang, X., Olson, J., Gopinath, K., Fan, T., Mao, H., 2013. Group independent component analysis and functional MRI examination of changes in language areas associated with brain tumors at different locations. PLoS One 8, e59657.
Whitfield-Gabrieli, S., Ford, J.M., 2012. Default mode network activity and connectivity in psychopathology. Annu. Rev. Clin. Psychol. 8, 49–76.
Zhang, H., Zuo, X.N., Ma, S.Y., Zang, Y.F., Milham, M.P., Zhu, C.Z., 2010. Subject order-independent group ICA (SOI-GICA) for functional MRI data analysis. NeuroImage 51, 1414–1424.
Zhou, I.Y., Liang, Y.X., Chan, R.W., Gao, P.P., Cheng, J.S., Hu, Y., So, K.F., Wu, E.X., 2014. Brain resting-state functional MRI connectivity: morphological foundation and plasticity. NeuroImage 84, 1–10.